Organic Microlaser Switches

International Edition: DOI: 10.1002/anie.201502684
German Edition: DOI: 10.1002/ange.201502684

Low-Threshold Wavelength-Switchable Organic Nanowire Lasers Based on Excited-State Intramolecular Proton Transfer**

*Wei Zhang, Yongli Yan, Jianmin Gu, Jiannian Yao, and Yong Sheng Zhao**

Abstract: *Coherent light signals generated at the nanoscale are crucial to the realization of photonic integrated circuits. Self-assembled nanowires from organic dyes can provide both a gain medium and an effective resonant cavity, which have been utilized for fulfilling miniaturized lasers. Excited-state intramolecular proton transfer (ESIPT), a classical molecular photoisomerization process, can be used to build a typical four-level system, which is more favorable for population inversion. Low-power driven lasing in proton-transfer molecular nanowires with an optimized ESIPT energy-level process has been achieved. With high gain and low loss from the ESIPT, the wires can be applied as effective FP-type resonators, which generated single-mode lasing with a very low threshold. The lasing wavelength can be reversibly switched based on a conformation conversion of the excited keto form in the ESIPT process.*

Organic micro/nanolasers have attracted great interest because of their promising applications ranging from high-throughput sensing to on-chip optical communication.[1] In recent years, organic nanowires with well-defined structures fabricated with epitaxial growth,[2] template methods,[3] vapor deposition,[4] electrospinning,[5] solution self-assembly,[6] drawing and nanopatterning,[7] and so on, have been demonstrated to be able to act as active gains and optical waveguide cavities for nanoscale lasers. In these organic nanomaterials, stimulated emission usually takes place from excited state $|10\rangle$ to the first vibronic replica $|01\rangle$ of the ground state, exhibiting a quasi-four-level process.[8] Because of the small Stokes shift induced by the quasi-level process, organic nanowires are subjected to severe re-absorption waveguiding loss, resulting in high lasing thresholds.[6a] Meanwhile, based on 0–1 gain transition in the quasi-level structure, the optical gain region of organic nanomaterials is limited,[3a] and unfit for the achievement of wide-gain emission, which is vital for the realization of wide-wavelength tunable lasers.[9] Hence, the development of a gain mechanism with real four-level structure that has large Stokes shift and multiple gain positions, is essential for the realization of low-threshold wide-gain tunable nanowire lasers.

Photoisomerization provides an effective way to overcome the above-mentioned problems because of the large spectral separation and possibly multiple emissive states between different isomers.[10] The isomerizations of some photochromic systems have been utilized to fulfil optical gains.[11] However, the photochromism is in fact not a transient reversible four-level photocycle between the two isomers, and the lasing therein is mainly based on the absorption and stimulated emission of one of the isomers, which is actually a quasi-four-level process built upon the vibronic progressions of the S_0 and S_1 states. In comparison, excited-state intramolecular proton transfer (ESIPT) is a fast photoisomerization process between the enol and keto excited states of intramolecularly hydrogen-bonded molecules. Accompanied with remarkable changes in molecular geometry and electronic structure, the ESIPT process favors the formation of a typical four-level structure, and leads to the large Stokes shifted fluorescence emission.[12]

Thus, the ESIPT molecules would exhibit higher gain and lower loss than common dyes, owing to their facile population inversion and negligible self-absorption.[10b] To date, most of the ESIPT-based stimulated emissions were mainly obtained in solution or amorphous films.[13] However, the ESIPT processes therein are often disturbed by the solvent or environment,[14] which would exhibit a less effective four-level process and thus result in relatively high density thresholds. Compared with the monomers or amorphous films, crystalline states with ordered and tight packing may show a more optimized ESIPT four-level process without disturbance,[15] as well as high gain density, low defect density, and strong self-cavity effects.[16] Therefore, crystalline nanostructures of ESIPT molecules could be applied to fabricate compact and miniaturized lasers of high performance. More importantly, the optimized four-level structure might show wide gain because of the multiple ESIPT excited states,[10b,17] which would provide a probability to realize wide-tunable nanowire lasers.

Herein, we propose an optimized ESIPT four-level structure to realize low-threshold lasing in proton-transfer molecular nanowires, where the existence and conversion of two keto excited states in the gain process were demonstrated and utilized to switch the lasing wavelength. The ESIPT molecular nanowires with well-defined crystal structures were designed and synthesized through a liquid-phase self-assembly method. In these nanowires, the formation of the *trans*-enol and *trans*-keto states were restricted by the tight molecular packing, leading to an effective ESIPT four-level process. The optimized energy-level process resulted in

[*] W. Zhang, Dr. Y. Yan, Dr. J. M. Gu, Prof. J. N. Yao, Prof. Y. S. Zhao
Beijing National Laboratory for Molecular Sciences (BNLMS)
Key Laboratory of Photochemistry, Institute of Chemistry
Chinese Academy of Sciences, Beijing 100190 (China)
E-mail: yszhao@iccas.ac.cn

[**] This work was supported by the National Natural Science Foundation of China (21125315, 21221002), the Ministry of Science and Technology of China (2012YQ120060), and the Strategic Priority Research Program of the Chinese Academy of Sciences (XDB12020300).

Supporting information for this article is available on the WWW under http://dx.doi.org/10.1002/anie.201502684.

intense *cis*-keto* emission and minimized the re-absorption, which are beneficial for the achievement of strong microcavity effects and low-threshold single-mode lasing. Moreover, we found that there is a reciprocal transformation between two different *cis*-keto* excited states in the peculiar ESIPT process via the conversion of the molecular conformation, which was subsequently utilized to build wavelength-switchable lasers by inducing the photoisomerization under highly stimulated emission. We believe the results demonstrated herein would help to better understand the lasing mechanism of organic dyes, and provide guidance for the development of miniaturized lasers with distinct functionalities.

2-(2′-hydroxyphenyl)benzothiazole (HBT, Figure 1 a) was selected as the model compound for the construction of the

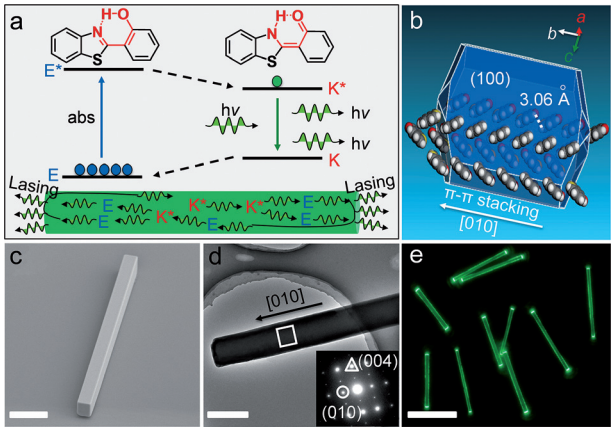

Figure 1. a) Illustration of ESIPT four-level gain process based on the enol–keto phototautomerization of a model compound HBT. b) Theoretically predicted growth morphology of a HBT crystal based on the attachment energies calculated with Material Studio package. The predicted growth thermodynamic stable morphology is 1D wire-like structure growing along the *b* axis. c) SEM image of a HBT nanowire with square cross-section and smooth face. Scale bar: 2 μm. d) TEM image of a single HBT nanowire. Scale bar: 1 μm. Inset: SAED pattern of the wire collected from the microarea marked with the white square. e) PL image of some discrete HBT wires excited with the UV band (330-380 nm) of a mercury lamp. Scale bar: 10 μm.

nanolasers owing to its typical ESIPT property and π-conjugated planar molecular configuration that will facilitate the assembly into regular-shaped crystalline microstructures.[10b,18] As shown in Figure 1 a, the ground-state HBT molecules exist as an *cis*-enol (E) form, while upon photoexcitation, the excited enol (E*) state quickly transfer to the *cis*-form excited keto (K*) state via the intramolecular proton transfer from the oxygen to the nitrogen atoms. The excited-state proton transfer is immediately followed by the radiative transition from K* to K, and then the rapid ground-state reverse proton transfer from K to E, which thereby builds a fast four-level photocycle (E-E*-K*-K-E). The four levels represent separate electronic states of two tautomers with drastically different molecular geometries and electronic structures, where the keto isomer has zero initial population at ground state, leading to an easy population inversion as well as large Stokes shifted emission from K*.[19] Combining the optical feedback, the first photon arising from the K* state would be continuously amplified by stimulated emission during the back-and-forth travelling without self-absorption, triggering an low-threshold lasing emission. Furthermore, from the thermodynamically stable molecular packing of HBT shown in Figure 1 b, we can see that the strong intermolecular π–π interaction would facilitate the crystal growth along a specific direction to form a one-dimensional (1D) nanostructure,[20] which can serve as Fabry–Pérot (FP) type microcavity resonators for the aforementioned gain amplification.

The HBT nanostructures were fabricated with a facile solution self-assembly method.[21] In a typical preparation, a stock solution (100 μL) of HBT (2 mM) in tetrahydrofuran was rapidly injected into 5 mL of water under stirring at 4 °C. The rapid change of the surroundings initiated the nucleation and self-assembly of HBT molecules. After aging for 60 min, HBT nanowires were obtained (see the Supporting Information). As shown in the SEM image in Figure 1 c, the as-prepared HBT nanostructures have well-defined 1D wire-like morphology with smooth and flat surfaces. The smooth surfaces would minimize the optical scattering loss, and the flat end facets (AFM image; Supporting Information, Figure S2) can efficiently reflect the guided K* emission, which is essential for the optical gain and amplification.[22] The XRD pattern of the nanowires (Supporting Information, Figure S3) verifies the high crystallinity of the nanowires. The TEM image and the corresponding selected-area electron diffraction (SAED) pattern in Figure 1 d indicate that the wire is a high-quality single crystal growing along the [010] direction, which is attributed to the preponderant molecular packing based on π–π interaction as shown in Figure 1 b. The single-crystal nanostructures would well improve the confinement of light, and facilitate effective optical waveguiding.[23] Under UV excitation, the HBT nanowires exhibit strong green photoluminescence (PL) from K* state with typical features of active optical waveguide, such as bright spots at the wire ends and weaker PL from the wire bodies (Figure 1 e). This feature suggests that the nanowires can absorb the UV light, and effectively propagate K* energy along the 1D axis direction, which is partially ascribed to the excellent crystalline nanostructures. Combining the characteristics of active optical waveguide and efficient reflection, the HBT nanowires may exhibit a strong microcavity effect, which is of great importance for the realization of lasing.[6a]

As compared with HBT monomers in solution, the crystalline state nanowires with close molecular packing can efficiently restrict the intramolecular *cis–trans* rotation between benzothiazole and hydroxyphenyl rings (Supporting Information, Figure S4), which is beneficial to avoid the formation of undesired *tans*-keto and *trans*-enol states (Supporting Information, Figure S5).[10b,24] As a result, the HBT nanowires exhibit a very strong *cis*-keto* emission with quantum yield $\Phi_{NWs} \approx 0.68$, much higher than that of the monomers in solution ($\Phi_M \approx 0.01$; Supporting Information, Figure S6), which indicates the occurrence of a more effective energy-level emission process. Moreover, the *cis*-keto* emission (ca. 514 nm) of the HBT nanowires exhibits a large Stokes shift from the *cis*-enol absorption (ca. 355 nm), which

is one of the superiorities of ESIPT based four-level system. The typical four-level process suggests the HBT nanowires could function as excellent gain media.

When a single HBT wire was excited locally with a focused pulse laser beam (355 nm, ca. 150 fs; Supporting Information, Figure S7), a strong green light waveguiding from excitation point to the end tips was observed (Figure 2a), revealing that

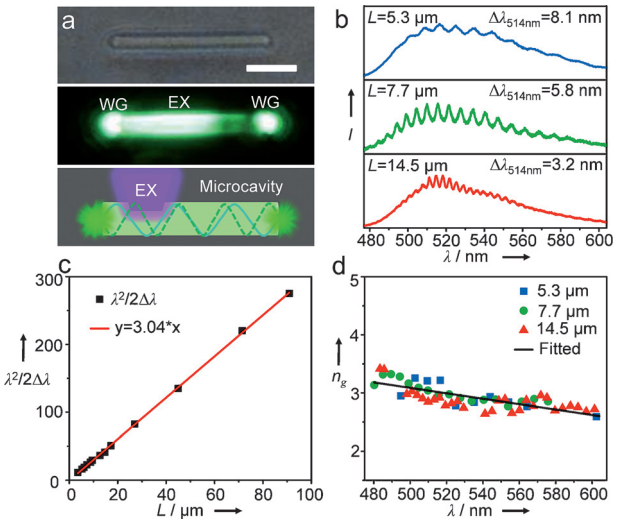

Figure 2. a) Bright-field (top) and PL (middle) images of a single HBT wire ($L = 14.5$ μm) excited with a pulsed laser (355 nm). EX: excited spot; WG: waveguided spot. Scale bar: 5 μm. Bottom: depiction of a nanowire waveguide, with cleaved ends defining a FP cavity. b) Modulated PL spectra collected at the guided tips of three HBT nanowires with different lengths. c) The plot and fitted curve of $\lambda^2/2\Delta\lambda$ ($\lambda = 514$ nm) versus the length of the wires. d) Group refractive index n_g versus wavelength.

the *cis*-keto* energy can be efficiently generated and propagated along the wire axis, and outcoupled from the tips. The light propagation exhibits a very small optical loss with coefficient of $\alpha \approx 33$ dB cm^{-1} at 514 nm (Supporting Information, Figure S8), which is much lower than those of common organic nanostructures.[25] The low waveguide loss can be ascribed to the peculiar molecular four-level photocycle with the large Stokes shift, which would be beneficial for an effective FP-type microcavity resonance.

The FP-type nanowire microcavity can support a standing-wave optical field between the two end facets, where the *cis*-keto* energy would travel back and forth (Figure 2a, bottom), leading to a discrete set of resonant modes in the PL spectra.[26] The resonantly modulated PL spectra were collected from the end tips of HBT wires with different lengths ($L = 5.3$, 7.7, 14.5 μm) to investigate the microcavity effects. As shown in Figure 2b, the modulated PL spectra present an increasing modes number with the increase of the cavity length. The mode spacing ($\Delta\lambda$) versus nanowire length (L) is in reasonable agreement with that given by the equation $\Delta\lambda = \lambda^2/2\,L\,n_g$,[3a] where n_g is the group refractive index as a function of wavelength. The linear relationship between $\lambda^2/2\Delta\lambda$ and the length of the nanowires (Figure 2c) indicates that the PL modulation is resulted from the axial FP-type cavity resonance.

Based on the linear fitting relationship in Figure 2c, the group refractive index n_g around 514 nm can be identified with a value of 3.04, which is high enough to induce the tight confinement of FP-type modes in the HBT nanowires with low optical leakage to substrates and air (Supporting Information, Figure S9). The group refractive index versus different wavelength plotted in Figure 2d presents a distinct dispersion relation that n_g is nearly constant around 3.0 over the entire emission regime. The dispersion relation is different from other organic aggregates that usually exhibit a rapidly increasing n_g within their absorption bands.[27] This indicates that it is nearly transparent for the *cis*-keto* energy to propagate in the ESIPT nanowires, which would induce a low microcavity loss with high quality (Q) factor. The Q factor was calculated to be over 1500 (Supporting Information, Figure S10), which is quite high for organic resonators.[28]

With the high-quality microcavity and efficient energy-level gain, HBT nanowire laser was achieved at low-power pulse excitation, as shown in Figure 3a. Below the lasing

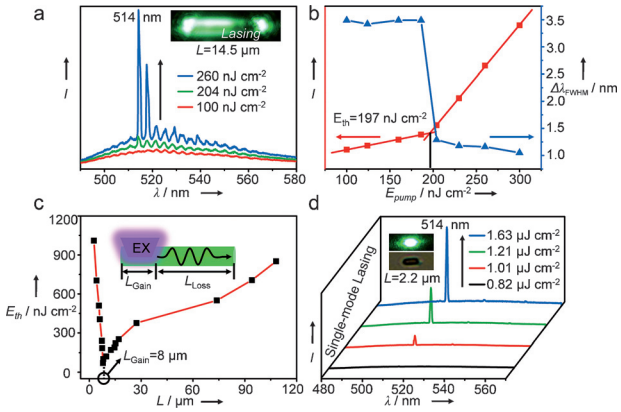

Figure 3. a) PL spectra recorded from the tip of a 14.5 μm long HBT nanowire excited with different energies. Inset: PL image of the wire above threshold. b) Power dependent profiles of PL intensities (red squares) and FWHM (blue triangles) around the mode peak 514 nm. c) Length-dependent lasing threshold profile. Inset: diagram of gain and loss in a single wire under local excitation. L_{Gain} and L_{Loss} are the length of gain and loss, respectively. d) Single-mode lasing from a 2.2 μm long nanowire. Inset: the lasing and bright-field images of the wire.

threshold, the PL spectrum collected from a single nanowire shows broad FP modes over the emission regime. When the pump fluence reaches about 200 nJ cm^{-2}, several mode peaks were selectively and strongly amplified. Above the onset power, the full-width at half-maximum (FWHM) at 514 nm dramatically narrows down to about 1 nm and the peak intensity increases rapidly and superlinearly with the pump fluence, which reveals a clear knee behavior and a threshold characteristic of a laser (Figure 3b). It is noted that the threshold of about 197 nJ cm^{-2} in HBT lasers is much lower than conventional organic microlasers.[2–7]

It is known that the lasing threshold strongly depends on both the optical gain and the loss process. Under local excitation, the lasing nanowire can be regarded as two distinct parts, the gain and loss regions, respectively (Figure 3c). The

gain and loss coefficients of a single wire should satisfy the equation $g_{th}L_{Gain} = \alpha L_{Loss} + \ln R^{-1}$,[29] where g_{th} is the threshold gain coefficient (proportionally to the lasing threshold), α is the coefficient of waveguide loss including substrate coupling loss and re-absorption loss, and R is the end facet reflectivity. According to the equation, the threshold would change along with the nanowire length. As shown in Figure 3c, for the longer wire ($L > 8$ μm), the lasing threshold decreases gradually with reducing length, owing to the decrease of the waveguide loss (L_{Loss}). As a result, a nanoscale laser with a very low threshold (ca. 70 nJ cm^{-2}) was achieved with an HBT wire of 8 μm long, which suggests a high-gain property of ESIPT molecular nanowires. The threshold turns to increase with the further decrease in the nanowire length owing to the decrease of the optical gain (L_{Gain}).

It can be seen that the very short nanowires can still function as effective FP-type laser resonators, providing an opportunity to achieve single-mode lasers which are important for signal processing and communicating to avoid the temporal pulse broadening and the false signaling.[30] It is known that the single-mode lasing can be obtained when the mode spacing exceeds the linewidth (ca. 18 nm; Supporting Information, Figure S11) of the gain region.[31] Based on the nanowire microcavity effects (Figure 2c), the $\Delta\lambda \approx 18$ nm can be achieved when the nanowire length decreases to about 2.5 μm. As shown in Figure 3d, a single-mode lasing around 514 nm, was successfully fulfilled in a 2.2 μm long nanowire. Moreover, the single-mode lasing action showed a relatively low threshold of about 1 μJ cm^{-2} in such a small size, further demonstrating the high gain and low loss in the HBT nanowires resulted from the peculiar ESIPT four-level process.

The HBT nanowires exhibit two strong *cis*-keto* emission regions; one band at about 514 nm and another at about 540 nm (Supporting Information, Figure S11). The distinguishing emission lifetimes for the two bands indicate the existence of two different fluorescent *cis*-keto* states (Supporting Information, Figure S12). Similarly to the *cis*-keto* species in salicylidene-aminopyridine solids,[32] the two excited states in HBT crystalline can be assigned to the planar (*cis*-keto$_1$*) and partially twisted (*cis*-keto$_2$*) fluorescent isomers (Figure 4a), respectively.[33] Under photoinduction, the high-energy *cis*-keto$_1$* generated from the ESIPT process may undergo either radiative decay with about 514 nm, or fast twisting to form the low-energy *cis*-keto$_2$* with an emission around 540 nm, as shown in the energy-level structure of the nanowires in Figure 4b.[34]

The conformation conversion between *cis*-keto$_1$* and *cis*-keto$_2$* can be utilized to realize a wavelength switching for the single-mode laser. As shown in Figure 4c, a single wire excited with a pump fluence of 4.5 μJ cm^{-2} exhibited a prominent lasing emission at 537 nm, indicating that the twisted *cis*-keto$_2$* state dominates the gain process, which is in sharp contrast with the lasing at 514 nm from the planar *cis*-keto$_1$* state in the same wire pumped with a lower fluence (2.4 μJ cm^{-2}). This means that high photoexcitation fluence would be beneficial to overcome the potential barrier for the excited state intramolecular twisting, and thus induce the generation and gain of the *cis*-keto$_2$*. Moreover, dual-wavelength lasing emission was achieved when a moderate pump fluence was employed, and the intensity ratio of the two lasing wavelengths (I_{537}/I_{514}) could be continuously tuned from about 0.1 to about 10 by varying the pump fluence, as illustrated in Figure 4d. This further testifies the existence and photoinduced conversion of the two *cis*-keto* excited states.

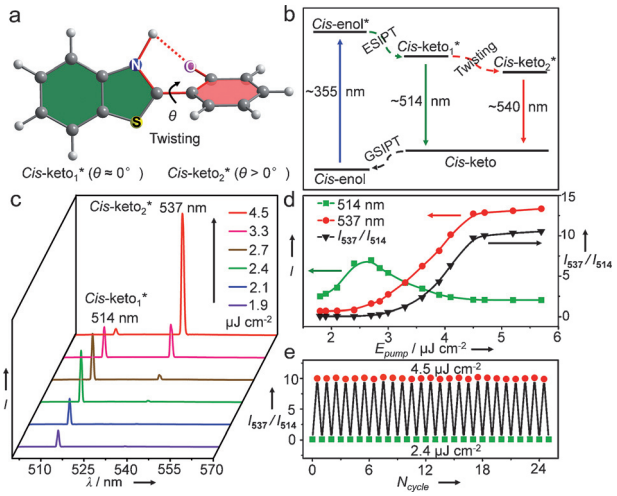

Figure 4. a) Planar (*cis*-keto$_1$*) and twisted (*cis*-keto$_2$*) keto excited states. θ is the twist angle between the benzothiazole ring and the hydroxyphenyl ring. b) ESIPT photocycle in the HBT nanowires with two *cis*-keto* states. GSIPT: ground-state intramolecular proton transfer. c) Lasing spectra of a 2.2 μm long nanowire excited with different energy above 1.8 μJ cm^{-2}. d) Power-dependent profiles of PL intensities around the mode peak 537 nm (red) and 514 nm (green), and the intensity ratio between two colors (black). e) Plot of the intensity ratio of 537 nm and 514 nm (I_{537}/I_{514}) against the switching cycles.

We then examined the reversibility and stability of the power-dependent wavelength-switchable lasing action. In each measurement, the pump fluence was kept at 2.4 μJ cm^{-2} for 1 min to obtain a single-mode lasing at 514 nm. The power was rapidly turned up to 4.5 μJ cm^{-2} to obtain a fast lasing wavelength switching to 537 nm, which was then held for another 1 min. After dozens of switching cycles, the I_{537}/I_{514} ratio remains nearly unchanged (ca. 0.1 at 2.4 μJ cm^{-2}, and ca. 10 at 4.5 μJ cm^{-2}), revealing good reproducibility and tolerance with low device fatigue. This excellent performance can be attributed to the ultrafast and reversible ESIPT four-level process,[10b] providing a new avenue to the realization of wide-wavelength tunable nanoscale lasers.

In summary, low-threshold organic nanowire lasers have been realized based on a typical excited-state intramolecular proton transfer (ESIPT) process. The tight molecular packing in the crystal nanowires restricted the formation of undesired excited states in the ESIPT, which was essential for the formation of an optimized four-level emissive process upon optical pump. The effective ESIPT four-level structure reduced the optical loss and favored the population inversion, which helped us to achieve a single-mode lasing under low pump energy. Furthermore, on the basis of a conformation conversion of the excited keto states in the ESIPT, we realized a single-wire laser switch via a photoinduced isomerization. The reported results would help us to fabricate nanoscale

lasers with specific functionalities through better understanding the population inversion processes, and to promote the advancement of self-assembled organic flexible optical elements into miniaturized photonic circuits with higher performances.

Keywords: excited-state intramolecular proton transfer · laser switch · nanophotonics · organic nanowire · nanowire laser

How to cite: *Angew. Chem. Int. Ed.* **2015**, *54*, 7125 – 7129
Angew. Chem. **2015**, *127*, 7231 – 7235

[1] a) S. R. Forrest, *Nature* **1999**, *397*, 294 – 295; b) Y. S. Zhao, H. Fu, A. Peng, Y. Ma, Q. Liao, J. Yao, *Acc. Chem. Res.* **2010**, *43*, 409 – 418; c) J. Yu, Y. Cui, H. Xu, Y. Yang, Z. Wang, B. Chen, G. Qian, *Nat. Commun.* **2013**, *4*, 2719; d) L. Persano, A. Camposeo, D. Pisignano, *Prog. Polym. Sci.* **2015**, *43*, 48 – 95.

[2] a) F. Quochi, F. Cordella, R. Orru, J. Communal, P. Verzeroli, A. Mura, G. Bongiovanni, A. Andreev, H. Sitter, N. Sariciftci, *Appl. Phys. Lett.* **2004**, *84*, 4454 – 4456; b) F. Quochi, *J. Opt.* **2010**, *12*, 024003.

[3] a) D. O'Carroll, I. Lieberwirth, G. Redmond, *Nat. Nanotechnol.* **2007**, *2*, 180 – 184; b) K. H. Cheng, Y. Zhong, B. Y. Xie, Y. Q. Dong, Y. Hong, J. Z. Sun, B. Z. Tang, K. S. Wong, *J. Phys. Chem. C* **2008**, *112*, 17507 – 17511.

[4] a) Y. S. Zhao, A. Peng, H. Fu, Y. Ma, J. Yao, *Adv. Mater.* **2008**, *20*, 1661 – 1665; b) S. M. Yoon, J. Lee, J. H. Je, H. C. Choi, M. Yoon, *ACS Nano* **2011**, *5*, 2923 – 2929.

[5] a) A. Camposeo, F. Di Benedetto, R. Stabile, A. A. Neves, R. Cingolani, D. Pisignano, *Small* **2009**, *5*, 562 – 566; b) A. J. Das, C. Lafargue, M. Lebental, J. Zyss, K. Narayan, *Appl. Phys. Lett.* **2011**, *99*, 263303; c) G. Morello, M. Moffa, S. Girardo, A. Camposeo, D. Pisignano, *Adv. Funct. Mater.* **2014**, *24*, 5225 – 5231.

[6] a) C. Zhang, C. L. Zou, Y. Yan, R. Hao, F. W. Sun, Z. F. Han, Y. S. Zhao, J. Yao, *J. Am. Chem. Soc.* **2011**, *133*, 7276 – 7279; b) Z. Xu, Q. Liao, Q. Shi, H. Zhang, J. Yao, H. Fu, *Adv. Mater.* **2012**, *24*, OP216 – 220.

[7] a) V. D. Ta, R. Chen, L. Ma, Y. J. Ying, H. D. Sun, *Laser Photonics Rev.* **2013**, *7*, 133 – 139; b) L. Persano, A. Camposeo, P. D. Carro, V. Fasano, M. Moffa, R. Manco, S. D'Agostino, D. Pisignano, *Adv. Mater.* **2014**, *26*, 6542 – 6547.

[8] I. D. W. Samuel, G. A. Turnbull, *Chem. Rev.* **2007**, *107*, 1272 – 1295.

[9] a) F. Qian, Y. Li, S. Gradecak, H. G. Park, Y. Dong, Y. Ding, Z. L. Wang, C. M. Lieber, *Nat. Mater.* **2008**, *7*, 701 – 706; b) X. Liu, Q. Zhang, J. N. Yip, Q. Xiong, T. C. Sum, *Nano Lett.* **2013**, *13*, 5336 – 5343.

[10] a) A. Bianco, S. Perissinotto, M. Garbugli, G. Lanzani, C. Bertarelli, *Laser Photonics Rev.* **2011**, *5*, 711 – 736; b) J. E. Kwon, S. Y. Park, *Adv. Mater.* **2011**, *23*, 3615 – 3642.

[11] a) D. Pisignano, E. Mele, L. Persano, A. Athanassiou, C. Fotakis, R. Cingolani, *J. Phys. Chem. B* **2006**, *110*, 4506 – 4509; b) L. Persano, E. Mele, A. Athanassiou, R. Cingolani, D. Pisignano, *Chem. Mater.* **2006**, *18*, 4171 – 4175.

[12] A. U. Khan, M. Kasha, *Proc. Natl. Acad. Sci. USA* **1983**, *80*, 1767 – 1770.

[13] a) S. Kim, S. Y. Park, I. Yoshida, H. Kawai, T. Nagamura, *J. Phys. Chem. B* **2002**, *106*, 9291 – 9294; b) K. Sakai, T. Tsuzuki, Y. Itoh, M. Ichikawa, Y. Taniguchi, *Appl. Phys. Lett.* **2005**, *86*, 081103; c) K. Y. Chen, C. C. Hsieh, Y. M. Cheng, C. H. Lai, P. T. Chou, *Chem. Commun.* **2006**, 4395 – 4397; d) J. C. Del Valle, R. Claramunt, J. Catalan, *J. Phys. Chem. A* **2008**, *112*, 5555 – 5565.

[14] A. P. Demchenko, K. C. Tang, P. T. Chou, *Chem. Soc. Rev.* **2013**, *42*, 1379 – 1408.

[15] S. Park, O. H. Kwon, S. Kim, S. Park, M. G. Choi, M. Cha, S. Y. Park, D. J. Jang, *J. Am. Chem. Soc.* **2005**, *127*, 10070 – 10074.

[16] X. Li, N. Gao, Y. Xu, F. Li, Y. Ma, *Appl. Phys. Lett.* **2012**, *101*, 063301.

[17] T. Mutai, H. Tomoda, T. Ohkawa, Y. Yabe, K. Araki, *Angew. Chem. Int. Ed.* **2008**, *47*, 9522 – 9524; *Angew. Chem.* **2008**, *120*, 9664 – 9666.

[18] Y. Yan, Y. S. Zhao, *Chem. Soc. Rev.* **2014**, *43*, 4325 – 4340.

[19] P. Chou, D. McMorrow, T. Aartsma, M. Kasha, *J. Phys. Chem.* **1984**, *88*, 4596 – 4599.

[20] a) D. Winn, M. F. Doherty, *AIChE J.* **2000**, *46*, 1348 – 1367; b) W. Yao, Y. Yan, L. Xue, C. Zhang, G. Li, Q. Zheng, Y. S. Zhao, H. Jiang, J. Yao, *Angew. Chem. Int. Ed.* **2013**, *52*, 8713 – 8717; *Angew. Chem.* **2013**, *125*, 8875 – 8879.

[21] a) Q. H. Cui, Y. S. Zhao, J. Yao, *Adv. Mater.* **2014**, *26*, 6852 – 6870; b) P. Hui, R. Chandrasekar, *Adv. Mater.* **2013**, *25*, 2963 – 2967; c) B.-K. An, S.-K. Kwon, S.-D. Jung, S. Y. Park, *J. Am. Chem. Soc.* **2002**, *124*, 14410 – 14415.

[22] M. H. Huang, S. Mao, H. Feick, H. Yan, Y. Wu, H. Kind, E. Weber, R. Russo, P. Yang, *Science* **2001**, *292*, 1897 – 1899.

[23] a) Q. Bao, B. M. Goh, B. Yan, T. Yu, Z. Shen, K. P. Loh, *Adv. Mater.* **2010**, *22*, 3661 – 3666; b) N. Chandrasekhar, R. Chandrasekar, *Angew. Chem. Int. Ed.* **2012**, *51*, 3556 – 3561; *Angew. Chem.* **2012**, *124*, 3616 – 3621.

[24] a) R. Hu, S. Li, Y. Zeng, J. Chen, S. Wang, Y. Li, G. Yang, *Phys. Chem. Chem. Phys.* **2011**, *13*, 2044 – 2051; b) J. Li, Y. Li, C. Y. Chan, R. T. Kwok, H. Li, P. Zrazhevskiy, X. Gao, J. Z. Sun, A. Qin, B. Z. Tang, *Angew. Chem. Int. Ed.* **2014**, *53*, 13518 – 13522; *Angew. Chem.* **2014**, *126*, 13736 – 13740.

[25] a) F. Di Benedetto, A. Camposeo, S. Pagliara, E. Mele, L. Persano, R. Stabile, R. Cingolani, D. Pisignano, *Nat. Nanotechnol.* **2008**, *3*, 614 – 619; b) Y. S. Zhao, P. Zhan, J. Kim, C. Sun, J. Huang, *ACS Nano* **2010**, *4*, 1630 – 1636.

[26] I. D. W. Samuel, E. B. Namdas, G. A. Turnbull, *Nat. Photonics* **2009**, *3*, 546 – 549.

[27] a) K. Takazawa, *J. Phys. Chem. C* **2007**, *111*, 8671 – 8676; b) K. Takazawa, J. Inoue, K. Mitsuishi, T. Takamasu, *Phys. Rev. Lett.* **2010**, *105*, 067401.

[28] a) X. Wang, Q. Liao, Q. Kong, Y. Zhang, Z. Xu, X. Lu, H. Fu, *Angew. Chem. Int. Ed.* **2014**, *53*, 5863 – 5867; *Angew. Chem.* **2014**, *126*, 5973 – 5977; b) H. Fang, J. Yang, J. Feng, T. Yamao, S. Hotta, H. B. Sun, *Laser Photonics Rev.* **2014**, *8*, 687 – 715.

[29] J. Li, C. Meng, Y. Liu, X. Wu, Y. Lu, Y. Ye, L. Dai, L. Tong, X. Liu, Q. Yang, *Adv. Mater.* **2013**, *25*, 833 – 837.

[30] a) Y. Xiao, C. Meng, P. Wang, Y. Ye, H. Yu, S. Wang, F. Gu, L. Dai, L. Tong, *Nano Lett.* **2011**, *11*, 1122 – 1126; b) H. Gao, A. Fu, S. C. Andrews, P. Yang, *Proc. Natl. Acad. Sci. USA* **2013**, *110*, 865 – 869; c) L. Feng, Z. J. Wong, R. M. Ma, Y. Wang, X. Zhang, *Science* **2014**, *346*, 972 – 975; d) Q. Zhang, G. Li, X. Liu, F. Qian, Y. Li, T. C. Sum, C. M. Lieber, Q. Xiong, *Nat. Commun.* **2014**, *5*, 4953.

[31] a) V. D. Ta, R. Chen, H. D. Sun, *Adv. Opt. Mater.* **2014**, *2*, 220 – 225; b) R. Chen, V. D. Ta, H. D. Sun, *Sci. Rep.* **2012**, *2*, 244.

[32] M. Sliwa, N. Mouton, C. Ruckebusch, S. Aloïse, O. Poizat, G. Buntinx, R. Métivier, K. Nakatani, H. Masuhara, T. Asahi, *J. Phys. Chem. C* **2009**, *113*, 11959 – 11968.

[33] W. E. Brewer, M. L. Martinez, P. T. Chou, *J. Phys. Chem.* **1990**, *94*, 1915 – 1918.

[34] a) M. Itoh, Y. Fujiwara, *J. Am. Chem. Soc.* **1985**, *107*, 1561 – 1565; b) M. Han, Y. Tian, Z. Yuan, L. Zhu, B. Ma, *Angew. Chem. Int. Ed.* **2014**, *53*, 10908 – 10912; *Angew. Chem.* **2014**, *126*, 11088 – 11092.

Received: March 23, 2015
Published online: April 29, 2015

